Journal of Metals, Materials and Minerals, 34(3), 1836, 2024

Comparative studies of radio transparency and dielectric characteristics of polymer composites

Azira YERMAKHANOVA[1], Aidar KENZHEGULOV[1,2,*], Berdiyar BAISERIKOV[1,3], Mohammed MEIIRBEKOV[1,3], and Nurlan BOGUSPAYEV[4]

[1] *National Center for Space Study and Technology JSC, Almaty city, Kazakhstan*
[2] *Satbayev University, Institute of Metallurgy and Ore Beneficiation JSC, Almaty city, Kazakhstan*
[3] *Satbayev University, Almaty city, Kazakhstan*
[4] *Limited Liability Partnership "Almaty Institute of Technology", Almaty city, Kazakhstan*

***Corresponding author e-mail**: a.kenzhegulov@satbayev.university

Received date:
7 September 2023
Revised date:
18 May 2024
Accepted date:
2 July 2024

Keywords:
Aramid-epoxy composite;
Fibreglass;
Dielectric permittivity;
Radio transparency;
Tangent angle

Abstract

Aramid-epoxy composites and glass fiber reinforced plastics are widely used in the manufacturing of the fairing design for modern aerospace vehicles due to their excellent mechanical properties combined with radio transparency in wave transfer. In this paper, aramid-epoxy composite and fiberglass were fabricated by the vacuum infusion method for a comparative study on radio transparency and dielectric characteristics. The radio transparency of the studied materials was evaluated by free-space measurements in the frequency range of 1 GHz to 8.5 GHz. According to the radio transparency results, the aramid-epoxy composite undergoes less electromagnetic wave loss than glass fiber reinforced plastic. Modifying the epoxy resin with tricresyl phosphate in aramid-epoxy resin leads to an increase in mechanical properties with a slight decrease in transmittance and a non-significant increase in dielectric characteristics. The dielectric characteristics results have demonstrated low values ($\varepsilon = 2.87$ and $\tan\delta = 0.037$) for aramid composites compared to fiberglass.

1. Introduction

One of the most critical elements of aircraft design, largely determining the aerodynamic characteristics and target accuracy, is the head antenna radome [1,2]. The problem of material selection for the fairing is a primary concern when creating a new design, so the most important physical and mechanical properties should be carefully analyzed. The material of the fairing should be not only strong but also radio transparent in the operating frequency range of the antenna [3-5].

Radio transparency is the ability of a material to transmit radio waves [6]. It is closely connected to the level of dielectric permittivity (ε) and dielectric loss tangent angle (tan δ). The lower the ε and tan δ, the lower the loss of the electromagnetic wave that is transmitted to the antenna through the fairing. Reducing dielectric permittivity (DP) and the dielectric dissipation factor can reduce capacitance and signal time delay, thus improving signal transmission quality in antennas and fairings [7,8]. All these factors set higher requirements for composite materials used in aircraft fairing design.

Polymer composite materials, particularly aramid-epoxy composite (AEC) and fiberglass (FG), are good candidates for fairing material selection due to their low dielectric properties and excellent mechanical properties. The complex properties of these composites mainly depend on the phase of the polymer matrix, the phase of the reinforcing fibers, and the fiber/polymer matrix interface [9-13]. A review of the literature reveals several studies focused on the dielectric permittivity and the tangent of the dielectric loss angle of AEC and FG. For the FG produced by LLC "Composite Technologies Ru," the dielectric permittivity ranges from 4 to 14, and the tangent of the dielectric loss angle is in the range of 0.01 to 0.05 [14]. Study [15] compares the dependence of dielectric permittivity on frequency. The research found that for aramid composites, the dielectric permittivity decreases from 3.48 to 3.4 with an increase in frequency from 8 GHz to 12 GHz. In the case of basalt composites, the dielectric permittivity increases from 3.75 to 3.97 with increasing frequency from 8 GHz to 12 GHz. According to reference [16], the dielectric permittivity of Kevlar (aramid) is approximately 3.5 to 4.5, confirming the presented information.

Recently, scientific literature indicates many articles [13,17-23] investigating the wave transparency and dielectric characteristics of aramid and glass epoxy composite materials, which are mainly obtained by vacuum forming, hot pressing, or resin casting methods. According to a review paper [13], the creation of radio-transparent composites with a polymer matrix with low ε and tan δ can be achieved either by reducing the polarization molecular density and polarization coefficient of reinforced fibers and polymer matrix or by increasing the strength of interfacial bonding of composites. In the [18] paper, a low-profile fairing was fabricated with an AEC face and foam core for low visibility. The dielectric constant and loss angle tangent of AEC measured by the free-space measurement method were 3.742 and 0.018, respectively. The maximum transmission rate was 83% at a 0.99 GHz bandwidth for a transmission rate greater than 80%. Under the supervision of

Choi I. and Chin W. [19,20], the authors used a free-space method to characterize hybrid composite low-visibility fairings with a sandwich construction consisting of E-glass/aramid/epoxy resin. The HF2 faceted hybrid composite barely visible fairing has met the performance requirements with a transmittance of 81% at the resonant frequency of 8.50 GHz and a bandwidth of 0.84 GHz. In the study [21], the authors investigated the dielectric parameters of unidirectional and quasi-isotropic AEC composites at different strains. According to the authors' results, DP increases by 0.045 at 0.001 strain. Additionally, the DP of quasi-isotropic composites is lower than that of unidirectional composites due to the different fiber orientations within the composite. The DP of epoxy composites increases with increasing filler content (Kevlar 49) and temperature. This is the conclusion reached by the authors [22]. In their view, the dielectric constant and losses of composites are mainly affected by interfacial polarization due to inhomogeneities at the interfaces introduced by the filler material. Xu X. *et al.* [23] have measured the dielectric properties of unidirectional AECs in the temperature range from room temperature to 200°C and concluded that both DP and losses increase with increasing temperature. The change in DP is linearly temperature dependent, while the change in dielectric loss is nonlinear.

However, even considering the above-mentioned research works on radio transparency and dielectric characteristics, this field requires further in-depth research on the radio transparency of composites. While studies on the mechanism of influence of epoxy resin (ER) modification on dielectric characteristics are still limited, they are absent on radio transparency. Pursuant thereto, the purpose of this work included a comparative study of radio transparency and dielectric characteristics of modified AEC and FG.

2. Experimental

In order to investigate the radio transparency and dielectric characteristics of the composites, two AEC samples and one FG sample were fabricated by the vacuum infusion method. A detailed description of the methodology is presented in our previous article [24]. The dielectric constant of the epoxy resin is 3.75. Table 1 demonstrates the physical properties of the obtained composites.

AEC-1 was made of L-grade epoxy resin (PoxySystems, Germany) with EPH hardener and Aramid 3300 dtex aramid fabric (Teijin, Netherlands).

AEC-2 was made of the same epoxy resin but modified with 10 wt% plasticizer tricresyl phosphate (TCP) and combined reinforcement of aramid fabric and aramid roving TWARON 805TEX (Teijin, Netherlands) (50% : 50%).

FG was made of the same epoxy resin and Ortex 360 $g \cdot m^{-2}$ to 300 $g \cdot m^{-2}$ glass fabric (Altair M LLC, Russia).

As can be seen from the table, the density of the composites depends on the density of the reinforcement material used, the epoxy resin, and the molding method. Since the same resin and molding method were used for all composites, the difference in density is related to the reinforcement materials used. Aramid fibers have a density of 1.44 $g \cdot m^{-3}$ and glass fibers 2.5 $g \cdot m^{-3}$. Undoubtedly, the density of the material affects radio transparency. Since one of the main objectives of this study was to compare the radio transparency characteristics depending on the reinforcement materials of the composites used, normalization work using density was not carried out.

2.1 Measurement of radio transparency

The dimensions of the AEC and FG samples were designed specifically for measuring radio transparency in an approximate A3 format, as shown in Figure 1. The measurements of dielectric characteristics of the AEC and FG samples were carried out using the measuring equipment at the Subsidiary of the limited liability partnership “Institute of Space Technique and Technology” (ISTT) in an anechoic screened chamber (ASC) by the free space measurement method. The measurements of the radio transparency of the material samples (electromagnetic transmission coefficient) were performed by comparing the electromagnetic radiation levels between the transmitting and receiving horn antennas in the presence of the sample and without it, as shown in Figure 2.

The equipment used in measuring the radio transparency of the material samples included:

Spectral analyzer N9010B Keysight (Keysight Technologies, United States) with EMI measuring receiver

Signal Generator N5071 waveform generator (Keysight Technologies, United States)

Horn antenna P6-23M/2 (MRIIE, Republic of Belarus)

The measurements were performed in the anechoic screened chamber.

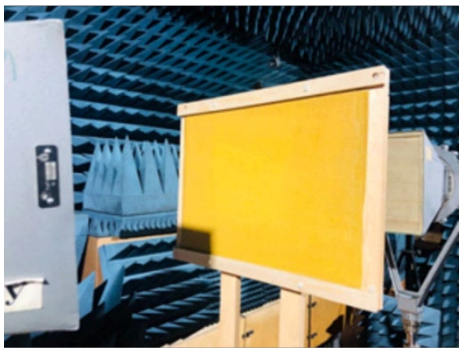

Figure 1. A3-size AEC sample.

Table 1. Physical properties of fibreglass and aramid-epoxy composites.

Name of sample	Thickness (mm)	Density ($g \cdot cm^{-3}$)	Component ratio (reinforcing/matrix) (%)	Strength (MPa)	Impact resistance ($kJ \cdot m^{-2}$)
AEC-1	2	1,41	65/35	423	402
AEC-2	2	1,38	65/35	710	475
FG	2	1,8	65/35	260	155

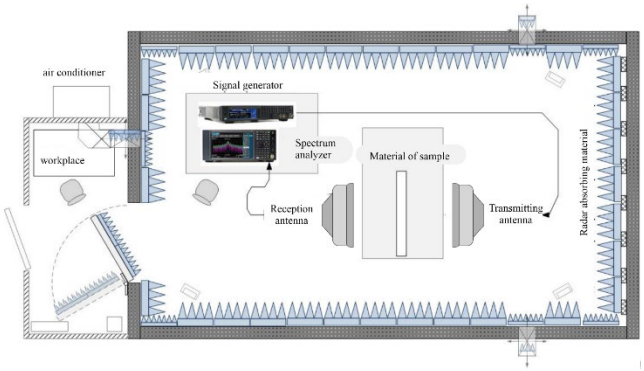

Figure 2. Measurement scheme for radio transparency of material sample in the ASC.

The radio transparency was measured in the frequency band of operation of the measuring horn antennas and devices, ranging from 1 GHz to 8.5 GHz. The measurable material sample in the setup had no contact with the antennas. The A3 sample area is 20% to 25% larger than the aperture area of the horn antennas, which agrees well with the measurement method, ensuring that the maximum electromagnetic energy in the antenna pattern passes through the sample instead of flowing between the antennas to bypass the sample.

During measurements within the frequency range of 1 GHz to 8.5 GHz, irregularities in the intrinsic transfer characteristic of the horn antennas were observed. To address this, the entire range was divided into three sections: 1 GHz to 4 GHz, 4 GHz to 6 GHz, and 6 GHz to 8.5 GHz for more accurate reporting of results. For each section, measurements were taken three times.

2.2 Measurement of dielectric characteristics

If dielectric permittivity (ε) characterizes the ability of a material to store energy in a dielectric compared to a vacuum (air), the dielectric (insulation) goodness factor (Q) characterizes the ability to store energy over time. Q is the ratio of stored energy to lost energy. In an alternating field, the total energy of the oscillating system will consist of the recharge energy and loss energy.

$$Q = \frac{E1}{E2} \quad (1)$$

where, E_1 – energy stored during one period, E_2 – energy lost during one period.

It is known that the quality of circuit in the presence of dielectric decreases by the value of losses in the dielectric medium. Accordingly, the t dielectric loss $tan\ \delta$ is the reciprocal value of Q [25,26]:

$$tan\ \delta = \frac{1}{Q} \quad (2)$$

Therefore, measuring the tuned circuit Q-factor with different dielectrics, we can calculate the losses of $tan\ \delta$.

The measurement of the tuned-circuit Q with the submitted materials was carried out by the resonator method in an alternating electromagnetic field using a FieldFox microwave analyzer N9915A (Keysight, USA). The oscillating circuit is formed by a quarter-wave λ/4 copper strip with dimensions of 70 mm × 6 mm × 0.5 mm, grounded at one end, and the walls of the resonating chamber with dimensions of 80 mm × 40 mm × 10 mm, made of aluminum D16. The samples of dielectric material are placed in the clearance between the strip and the bottom of the resonating chamber. This design of the resonating chamber is convenient for measuring flat specimens. The tight pressing of the copper strip to the sample is achieved by means of space fillers made from pieces of plastic with a small dielectric constant (ε) and small intrinsic losses (tan δ), such as foam plastic, under the lid of the resonating chamber as shown in Figure 3(a) and Figure 3(b).

Since the submitted samples have sufficient dielectric permittivity ($\varepsilon \geq 3$), a significant part of the electromagnetic field is concentrated in the dielectric, i.e., in the clearance between the strip and the bottom. The electromagnetic field above the strip is scattered, so the shielding cover of the resonating chamber affects the measurements insignificantly. The input and output of electromagnetic energy to the chamber are chosen to be inductive, ensuring that the capacitive properties of the dielectrics do not introduce distortion to the input and output elements.

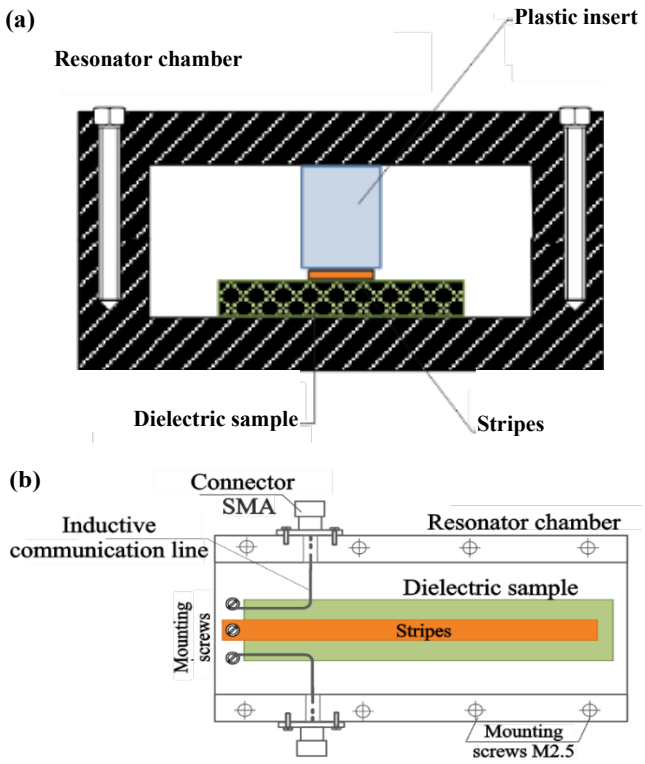

Figure 3. Resonating chamber, (a) end view, and (b) top view without cover.

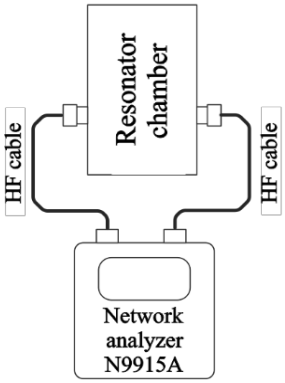

Figure 4. Measurement design of resonance Q factor.

The submitted samples had the same thickness of 2 mm. To maintain the tight clamping of the strip to the dielectric samples, its grounding is achieved by a screw method with the selection of the necessary height, and foam inserts of different sizes are prepared. The Q-factor of the obtained resonator with dielectric is observed by the amplitude-frequency response (AFR) of the circuit analyzer. The measurement design of the resonance Q factor is presented in Figure 4.

The measurements of dielectric permittivity of the samples were carried out by the condenser-type method described in [27]. The capacitance of the capacitor in the presence of AEC and FG composites and without them was measured with an APPA701 LCR meter (ARRA, Taiwan). DP shows how many times the electrical capacity C of the capacitor, between the liners of which there is a dielectric with DP ε, is greater than the electrical capacity C_{air} of the capacitor, between the liners of which there is a vacuum (or air, with dielectric permittivity ε = 1), using the formula 3:

$$\varepsilon = \frac{C}{C_{air}} \tag{3}$$

For mechanical clamping of the AEC and FG sheets between the capacitor plates (electrodes), a stand with electrodes made of D16 aluminum (size 170 mm × 138 mm) was constructed using precision milling vises with minimal microscrew backlash. In the stand, electrode insulators from the vise mechanism are made of caprolon material with low intrinsic DP to minimize the parasitic capacitance of the stand affecting the result. Three sample measurements were performed for each composite, followed by averaging.

3. Results and discussion

3.1 Study of samples radio transparency

Figure 5 shows one of three measurements of the electromagnetic field attenuation of the AEC-1 sample at the examined 1 GHz to 4 GHz, 4 GHz to 6 GHz, and 8 GHz to 8.5 GHz (screenshot). Trace 2 in blue is the background of the transmission coefficient of antennas with AEC-1 sample in air, track 1 yellow without sample. 1, 3, and 5 markers correspond to yellow trace 1, and markers 2, 4, and 6 correspond to blue trace 2 with sample. The comparisons should be made on markers located at the same or closely spaced frequencies: 1 and 2, 3 and 4, 5 and 6.

For example, in Figure 5, for the frequency interval 1 GHz to 4 GHz, marker 1 corresponds to frequency f = 1.230 GHz and attenuation 23.18 dBm, and marker 2 has a frequency of 1.240 GHz and attenuation 23.49 dBm. A difference in attenuation due to material losses: 23.49 – 23.18 = 0.31 dBm. Therefore, electromagnetic energy loss in AEC-1 at this frequency was 0.31 dBm. For the other frequencies, the calculation was performed similarly. In total, three values of electromagnetic energy loss in AEC-1 (0.147, 0.103, 0.353) were calculated, from which a mean value of ~0.20 dBm was derived.

According to the results of averaging three measurements of radio transparency for each AEC-1 frequency interval, it was determined that the attenuation is in the range of: 1 GHz to 4 GHz ~ 0.20 dBm, 4 GHz to 6 GHz ~ 0.73 dBm, 8 GHz to 8.5 GHz ~ 0.55 dBm.

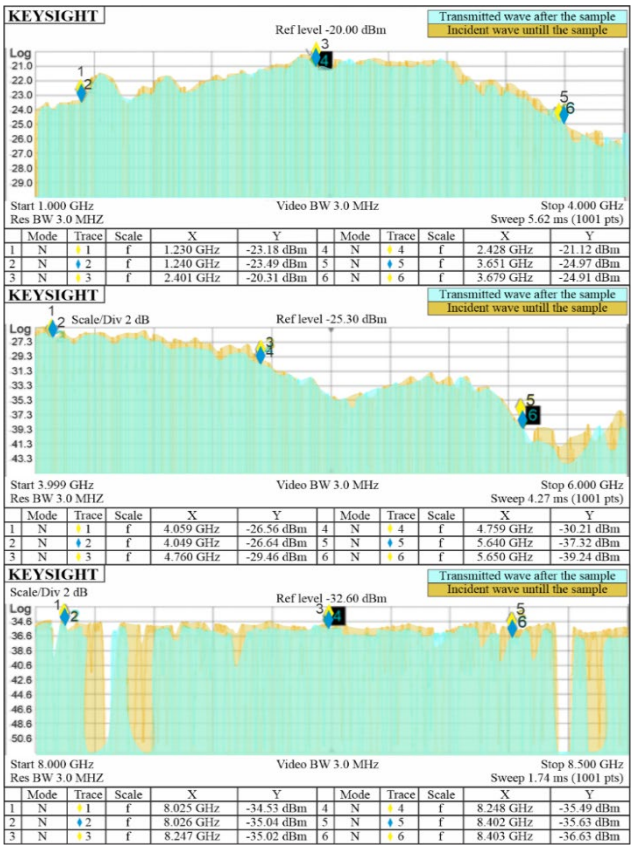

Figure 5. Measurement of field weakening in AEC-1.

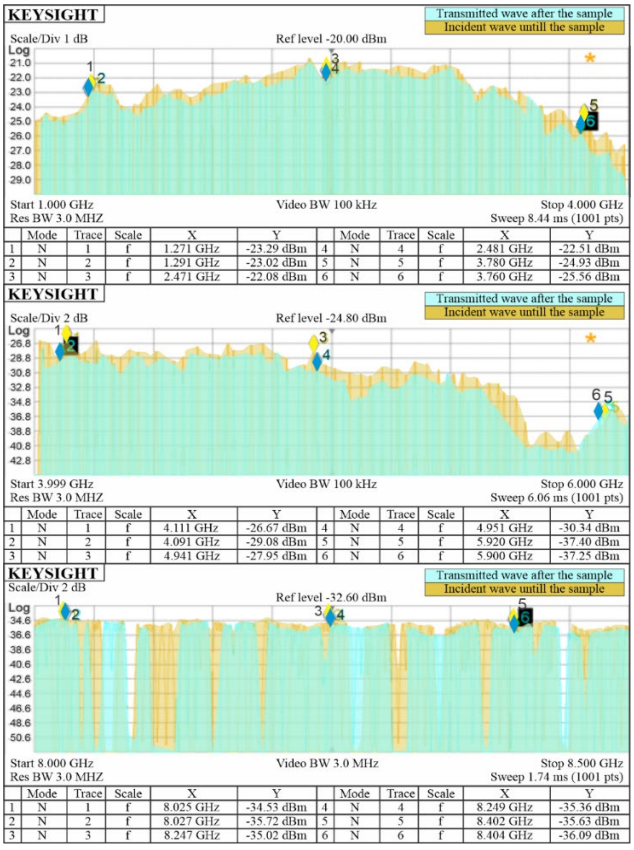

Figure 6. Measurement of field weakening in AEC-2.

Table 2 demonstrates the results of attenuation calculations followed by the deduction of the average value for each measurement frequency interval with respect to the AEC-1 composite.

The resulting average attenuation values of 0.20 dBm, 0.73 dBm, and 0.55 dBm can be converted to power ratios [28]. According to the voltage, current, and power ratio conversion table, 0.2 dBm corresponds to a power ratio of 0.955 (part of the power that has passed through the material). As a result, 0.955 represents 95.5% of the power that went through the material. The power loss in the material in the range of 1 GHz to 4 GHz is determined as follows: 100% – 95.5% = 4.5%.

In the case of measurement in the range 4 GHz to 6 GHz, the power loss of 0.73 dBm can be represented as 0.7 + 0.03 dBm. Then, 0.7 dBm corresponds to a power ratio of 0.8511 dBm, and 0.03 dBm corresponds to a power ratio of 0.9931. As a result, 0.8511 × 0.9931 = 0.8452, meaning 84.52% of the power passed through the material. The power loss in the material is 15.48% in the range 4 GHz to 6 GHz.

Similarly, a power loss of 0.55 dBm (at the frequency range of 8 GHz to 8.5 GHz) can be represented as 0.5 + 0.05 dBm. Then, 0.5 dBm corresponds to a power ratio of 0.8913 dBm, and 0.05 dBm corresponds to a power ratio of 0.9886. As a result, 0.8913 × 0.9886 = 0.8811, meaning 88.11% of the power passed through the material. The power loss in the material is 11.89% in the range 8 GHz to 8.5 GHz.

Therefore, the average radio transparency for AEC-1 across the three measurement ranges of 95.5%, 84.52%, and 88.11% is 89.4%.

Further, Figure 6 shows one of three measurements of the electromagnetic field attenuation of the AEC-2 sample in the examined 1 GHz to 4 GHz, 4 GHz to 6 GHz, and 8 GHz to 8.5 GHz ranges (screenshot). Similar calculations for determining radio transparency are performed for the AEC-2 composite. According to the results of averaging three measurements of radio transparency for each AEC-2 frequency interval, it is determined that the attenuation is in the range of: 1 GHz to 4 GHz ~ 0.42 dBm, 4 GHz to 6 GHz ~ 1.21 dBm, 8 GHz to 8.5 GHz ~ 0.31 dBm.

Table 3 shows the results of the attenuation calculations followed by the deduction of the mean value for each measurement frequency interval with respect to the AEC-2 composite. According to the ratio conversion table [28], attenuations of 0.42 dBm, 1.21 dBm, and 0.31 dBm correspond to power ratios of 0.907, 0.739, and 0.931, respectively.

In this manner, the average radio transparency for AEC-2 across the three measurement ranges of 90.7%, 73.9%, and 93.1% is 85.9%.

Next, Figure 7 shows one of three measurements of the attenuation of the electromagnetic field of the FG sample in the investigated 1 GHz to 4 GHz, 4 GHz to 6 GHz, and 8 GHz to 8.5 GHz ranges (screenshot). For the FG composite, similar calculations for determining the radio transparency were carried out. According to the results of averaging three measurements of radio transparency for each FG frequency interval, it was determined that the attenuation is in the range of: 1 GHz to 4 GHz ~ 0.3 dBm, 4 GHz to 6 GHz ~ 0.52 dBm, 8 GHz to 8.5 GHz ~ 1.85 dBm.

Table 4 specifies the results of attenuation calculations followed by the deduction of the average value for each measurement frequency interval with respect to the FG composite. According to the ratio conversion table [28], attenuations of 0.3 dBm, 0.52 dBm, and 1.85 dBm correspond to power ratios of 0.933, 0.887, and 0.653, respectively.

Therefore, the average radio transparency for FG across the three measurement ranges of 93.3%, 88.7%, and 65.3% is 82.4%.

Table 2. Indicators of field attenuation in AEC-1 in all frequency ranges.

Measurement	Blue marker frequency (dBm)	Yellow marker frequency (dBm)	Difference in attenuation (dBm)	Averaging (dBm)	Total electromagnetic energy loss (dBm)
	23.53	23.18	0.35		
1	20.46	20.31	0.15	0.147	
	24.91	24.97	-0.06		
	23.47	23.18	0.29		0.2
2	20.40	20.31	0.09	0.103	(at 1 GHz to 4 GHz range
	24.90	24.97	-0.07		frequency)
	23.49	23.18	0.31		
3	21.12	20.31	0.81	0.353	
	24.91	24.97	-0.06		
	26.45	26.56	-0.11		
1	30.31	29.46	0.85	0.917	
	39.33	37.32	2.01		
	26.74	26.56	0.18		0.73
2	29.81	29.46	0.35	0.360	(at 4 GHz to 6 GHz range
	37.87	37.32	0.55		frequency)
	26.64	26.56	0.08		
3	30.21	29.46	0.75	0.917	
	39.24	37.32	1.92		
	34.83	34.53	0.3		
1	35.36	35.02	0.34	0.330	
	35.98	35.63	0.35		
	35.47	34.53	0.94		0.55
2	35.64	35.02	0.62	0.670	(at 8 GHz to 8.5 GHz
	36.08	35.63	0.45		range frequency)
	35.04	34.53	0.51		
3	35.49	35.02	0.47	0.660	
	36.63	35.63	1		

Table 3. Indicators of field attenuation in AEC-2 in all frequency ranges.

Measurement	Blue marker frequency (dBm)	Yellow marker frequency (dBm)	Difference in attenuation (dBm)	Averaging (dBm)	Total electromagnetic energy loss (dBm)
	23.74	23.29	0.45		
1	22.34	22.08	0.26	0.490	
	25.69	24.93	0.76		
	23.04	23.29	-0.25		0.42
2	22.5	22.08	0.42	0.370	(at 1 GHz to 4 GHz range
	25.87	24.93	0.94		frequency)
	23.02	23.29	-0.27		
3	22.51	22.08	0.43	0.397	
	25.96	24.93	1.03		
	28.5	26.67	1.83		
1	29.46	27.95	1.51	1.467	
	38.46	37.4	1.06		
	29.18	27.36	1.82		1.21
2	30.61	30.21	0.4	1.677	(at 4 GHz to 6 GHz range
	41.28	38.47	2.81		frequency)
	28.65	27.78	0.87		
3	31.44	30.21	1.23	0.510	
	37.9	38.47	-0.57		
	34.28	34.53	-0.25		
1	34.96	35.02	-0.06	0.123	
	36.31	35.63	0.68		
	35.18	34.53	0.65		0.31
2	35.02	35.02	0	0.487	(at 8 GHz to 8.5 GHz
	36.44	35.63	0.81		range frequency)
	34.72	34.53	0.19		
3	35.36	35.02	0.34	0.330	
	36.09	35.63	0.46		

Table 4. Indicators of field attenuation in FG in all frequency ranges.

Measurement	Blue marker frequency (dBm)	Yellow marker frequency (dBm)	Difference in attenuation (dBm)	Averaging (dBm)	Total electromagnetic energy loss (dBm)
	24.16	24.24	-0.08		
1	21.7	21	0.7	0.450	
	23.6	22.87	0.73		
	24.25	24.24	0.01		0.3
2	20.87	21	-0.13	0.177	(at 1 GHz to 4 GHz range
	23.52	22.87	0.65		frequency)
	24	24.24	-0.24		
3	21.7	21	0.7	0.287	
	23.27	22.87	0.4		
	26.97	27.36	-0.39		
1	28.99	30.21	-1.22	-0.620	
	38.22	38.47	-0.25		
	29.18	27.36	1.82		0.52
2	30.61	30.21	0.4	1.677	(at 4 GHz to 6 GHz range
	41.28	38.47	2.81		frequency)
	28.65	27.78	0.87		
3	31.44	30.21	1.23	0.510	
	37.9	38.47	-0.57		
	36.7	34.53	2.17		
1	36.5	35.02	1.48	1.473	
	36.4	35.63	0.77		
	35.63	34.53	1.1		1.85
2	37.16	35.02	2.14	1.663	(at 8 GHz to 8.5 GHz
	37.38	35.63	1.75		range frequency)
	37.2	34.53	2.67		
3	37.41	35.02	2.39	2.413	
	37.81	35.63	2.18		

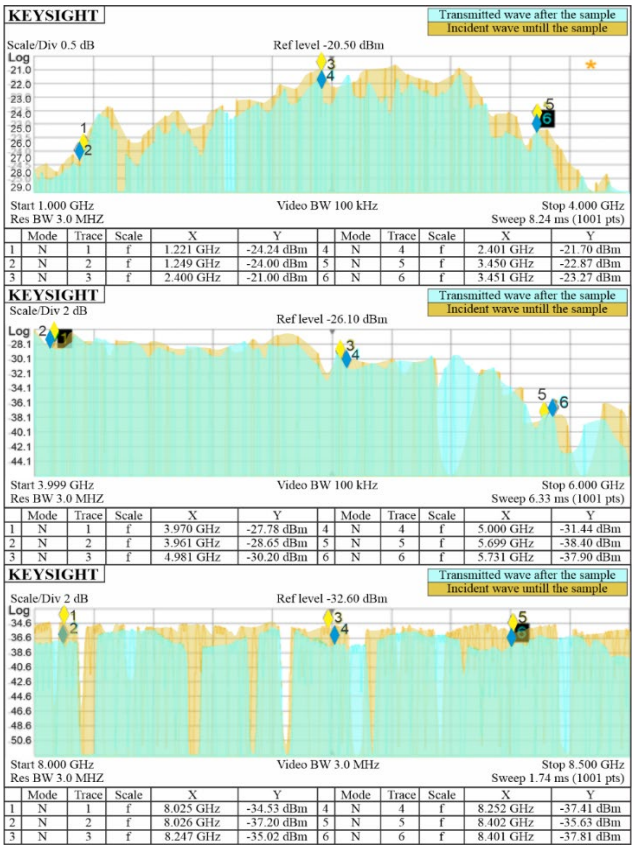

Figure 7. Measurement of field weakening in the FG.

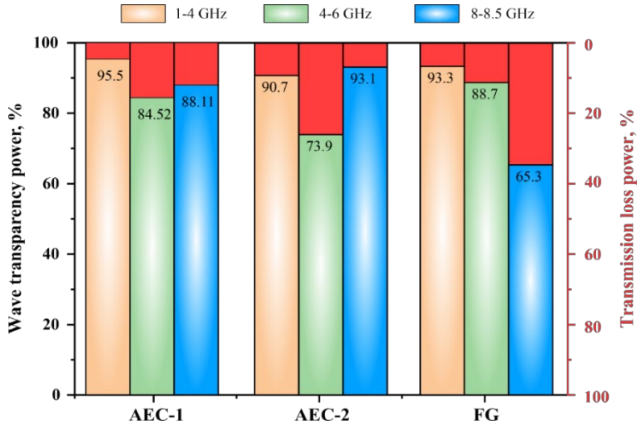

Figure 8. Transparent and lost wave power in AEC-1, AEC-1 and FG composites.

For the purpose of comparative study of radio transparency, the obtained data for all composites (AEC-1, AEC-2, and FG) are presented in Figure 8 for three measurement ranges. Red indicates the power loss during transmission in percent. As seen from the results, if we average the values among the investigated materials, AEC-1 has the highest radio transparency because a higher percentage of the wave's power has passed through it.

It is worth noting that the modification of ER with TCP leads to an increase in mechanical properties with minimal decrease in radio transparency in the measured frequency ranges. This is most probably due to the modifying effect of TCP. Since TCP is part of AEC-2, it affects the overall polarization and slightly increases the dielectric parameters. Additionally, the radio transparency of AEC composites is higher than that of FG. One of the main reasons is the lower DP of AEC composites compared to FG. It is known that the wave transmission characteristics of wave-transparent composites with a polymer matrix are usually evaluated by DP [9,29]. Unlike AEC, FG is made from glass fiber, which has a higher DP. Consequently, FG absorbs more radio waves, resulting in a decrease in its radio transparency compared to AEC.

Thus, the density of the composites depends on the density of the reinforcement material used, the epoxy resin, and the molding method. Since the same resin and molding method were used for all composites, the difference in density is related to the reinforcement materials used. Aramid fibers have a density of 1.44 g·cm^{-3} and glass fibers have a density of 2.5 g·cm^{-3}. Undoubtedly, the density of the material affects radio transparency. Since one of the main objectives of this study was to compare the radio transparency characteristics depending on the reinforcement materials of the composites used, normalization work using density was not carried out.

3.2 Investigation of dielectric properties

The dielectric permittivity (ε) and dielectric loss tangent angle (tan δ) are among the parameters that determine the wave transmission characteristics of radio-transparent polymer matrix composites [13, 29]. ε can characterize the polarization of composites, representing the ratio of a capacitor's capacitance with dielectrics to its capacitance in a vacuum [30]. Dielectric absorption loss means that when passing through the medium, a part of the electromagnetic wave is consumed and converted into heat energy [31]. In other words, the smaller the tanδ, the more the electromagnetic wave passes through the composite, increasing its radio transparency. The comparison of the results of the study of dielectric characteristics of the samples enables the comparison of the wave transmission characteristics of radio-transparent polymer matrix composites.

3.2.1 Study of samples dielectric losses

The dielectric losses in the investigated composites AEC-1, AEC-2, and FG have been measured using the dielectric Q factor, which was observed from AFR. The central resonance frequency is marked by marker 2 on the top of the AFR plot, and markers 1 and 3 are spaced left and right at the minus 3 dB level. The frequency difference between markers 1 and 3 (Δf) is the bandwidth. From [25,26], it is known that the resonance quality Q is calculated as follows:

$$Q = \frac{fcent}{\Delta f} = \frac{f\,cent}{f3\text{-}f1} \qquad (4)$$

The central resonance frequency f_{cent} depends on the dielectric permittivity, so it varies from sample to sample. The Q quality factor affects the bandwidth (Δf). The wider the Δf, the worse the Q factor, which means there are more dielectric losses (tanδ) in the material. After determining the Q factor, the value of tanδ was calculated using formula 2.

Figure 9 shows one of the three AFR measurements for AEC-1 (screenshot). The data comparison was also performed using three markers at different frequencies f_1, f_2, and f_3. Table 5 summarizes the results of loss angle tangent measurements in AEC-1.

Figure 10 shows the AFR of AEC-2. Table 6 summarizes the results of loss tangent measurements in AEC-2.

Further, Figure 11 shows the AFR of FG. Table 7 shows the results of loss tangent measurements in FG.

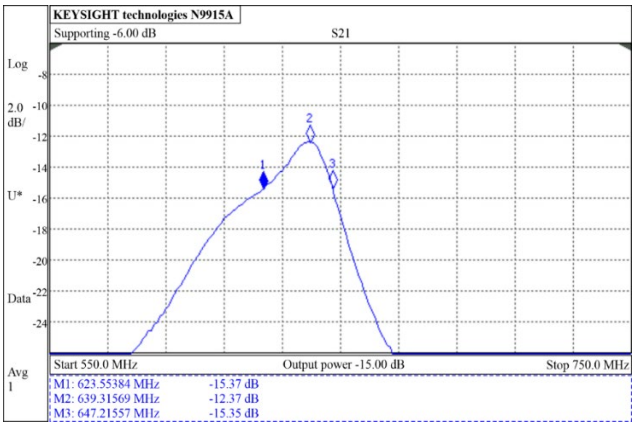

Figure 9. AFR of AEC-1.

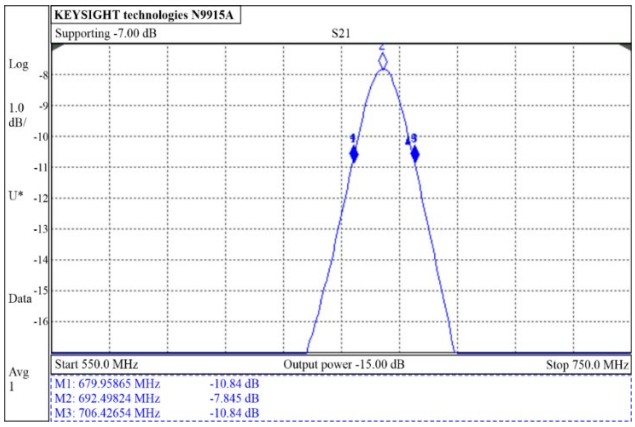

Figure 10. AFR of AEC-2.

Table 5. Results of loss angle tangent measurements in AEC-1.

Measurement	Frequency (MHz)	$Q = f_2/(f_3 - f_1)$	Tg = 1/Q	Average
1	f_1 = 623.55 f_2 = 639.31 f_3 = 647.21	27.02	0.0370	0.0372
2	f_1 = 625.61 f_2 = 640.43 f_3 = 649.31	27.02	0.0370	
3	f_1 = 624.52 f_2 = 640.43 f_3 = 648.62	26.56	0.0376	

Table 6. Results of loss tangent measurements in AEC-2.

Measurement	Frequency (MHz)	$Q = f_2/(f_3 - f_1)$	Tg = 1/Q	Average
1	f_1 = 679.96 f_2 = 692.49 f_3 = 706.43	26.14	0.0382	0.0381
2	f_1 = 679.09 f_2 = 691.58 f_3 = 705.54	26.02	0.0384	
3	f_1 = 682.02 f_2 = 695.00 f_3 = 708.23	24.45	0.0378	

Table 7. Results of loss tangent measurements in FG.

Measurement	Frequency (MHz)	$Q = f_2/(f_3 - f_1)$	Tg = 1/Q	Average
1	f_1 = 655.24 f_2 = 670.24 f_3 = 686.44	21.48	0.0465	0.0464
2	f_1 = 655.72 f_2 = 670.24 f_3 = 686.79	21.57	0.0463	
3	f_1 = 653.97 f_2 = 669.61 f_3 = 685.04	21.55	0.0464	

Table 8. Results of DP of AEC material and FG.

Sample	C_{diel}, picofarad	C_{air}	d_0 (mm)	ε	Averaged value ε
AEC-1	273	99.1	2	2.754	
AEC-1	286	97.6	2	2.930	2.874
AEC-1	289	98.3	2	2.939	
AEC-2	331	110.8	2	2.987	
AEC-2	333	110.7	2	3.008	3.003
AEC-2	335	111.1	2	3.015	
FG	600	129.4	2	4.636	
FG	597	135.6	2	4.403	4.58
FG	602	127.6	2	4.702	

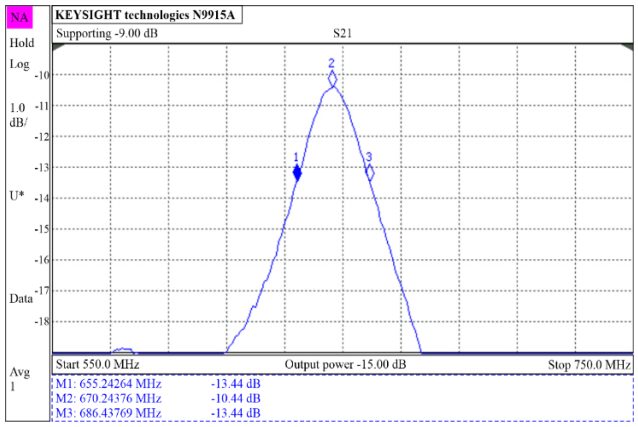

Figure 11. AFR of FG.

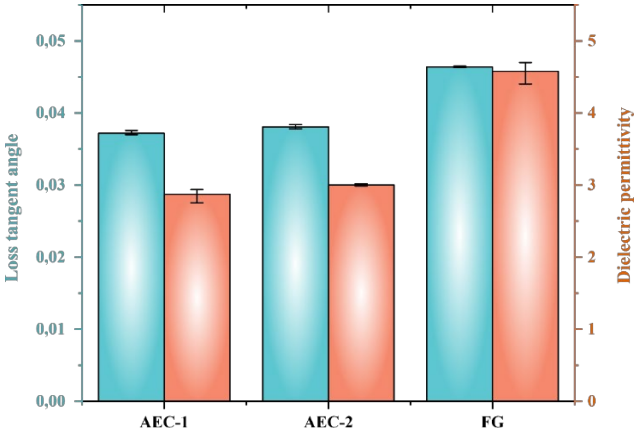

Figure 12. Dielectric permittivity ε at a current frequency of 1 kHz and dielectric loss tangent angle tanδ in the frequency range 550 MHz to 750 MHz of the obtained composites.

3.2.2 Study of samples dielectric permittivity

Table 8 summarizes the results of three measurements of AEC-1, AEC-2, and FG composites. As can be seen from the results, AEC-1 and AEC-2 have a mean DP of 2.874 and 3.003, respectively, whereas FG has a mean DP of 4.58. The obtained results for FG coincide with the reference data given in [25,27]. Due to the lower DP of aramid fiber compared to that of glass fiber, AEC composites demonstrate comparatively low values. One of the reasons for the difference in DP between AEC and FG composites is their structure. FG is composed of glass fibers, which have a higher DP than the polymeric materials used in AEC. Additionally, the moisture content and other impurities in the material are important factors affecting the DP. However, it should be realized that DP depends on many factors and can vary over a wide range depending on the specific material and operating conditions.

As it appears from the presented dielectric loss and DP data, they correlate with the previous free space analysis (radio transparency results). According to the impedance matching theory [32], the larger the ε of the medium, the stronger the electromagnetic wave is reflected, thereby reducing the efficiency of electromagnetic wave transmission through the material [33,34]. Figure 12 shows the comparative measurement results of dielectric permittivity (ε) and dielectric loss tangent angle (tanδ) of AEC-1, AEC-2, and FG composites. It should be noted in the comparison that the AEC-1 composite is characterized by low values of ε and tanδ, which contribute to an increase in transmittance or radio transparency. In the AEC-2 composite, a slight increase in ε and tanδ is observed due to the introduction of the tricresyl phosphate modifier into the ER.

4. Conclusions

In this work, aramid-epoxy composite and fiberglass were fabricated by the vacuum infusion method. Comparative studies of radio transparency and dielectric characteristics of the composites have been carried out. The radio transparency of the examined materials was evaluated by free space measurements in the frequency ranges of 1 GHz to 4 GHz, 4 GHz to 6 GHz, and 8 GHz to 8.5 GHz. According to the results of radio transparency, it can be concluded that the losses in the aramid-epoxy composite are less than those in fiberglass due to the lower dielectric constant and dielectric loss. Based on the averaged values, the transmission coefficients for AEC-1, AEC-2, and FG were 89.4%, 85.9%, and 82.4%, respectively. The dielectric characteristics for AEC-1 and AEC-2 aramid composites are lower compared to FG. In the AEC-2 composite, a slight increase in ε and tanδ is observed due to the introduction of the modifier into the epoxy resin, which contributed to a slight decrease in radio transparency.

Our results suggest that the comparative results of radio transparency and dielectric characteristics of glass and aramid-epoxy composites with changes in binder composition lead to different physical properties, including their radio transparency. By analyzing the results obtained in this work, aramid-epoxy composite-1 with dielectric permittivity of 2.87, dielectric loss of 0.03, and transmittance of 89.4% can be a candidate for fairing material in aerospace vehicles.

Acknowledgements

This work was supported by by the Science Committee of the Ministry of Education and Science of the Republic of Kazakhstan (grant No. AR09058225). The authors are grateful to Chief Engineer of LLP «Institute of Space Engineering and Technology» Samsonenko A.I. for analyzing the samples.

References

[1] D. A. Rogov, S. I. Latysh, and M. V. Vasyukov, "Development and design choice of ceramic rocket fairing and metal bulkhead joint," *Development*, vol. 22.2, pp. 94-102, 2015.

[2] M. Yu Rusin, *Design of rocket nose fairings made of ceramic and composite materials.* Moscow: Publishing house of MSTU im. N.E. Bauman, 2005.

[3] A. G. Romashin, V. E. Gaidachuk, Ya. S. Karpov, and M. Yu. Rusin, *Radiotransparent fairings for aircraft. Design, construction materials, production technology, testing.* Kharkov: Nat. aerospace un-t “Khark. aviation in-t", 2003.

[4] J. D. Kraus, and R. J. Marhefka, *Antennas for all applications*. NY: McGraw-Hill, 2003.

[5] M. N. Meyirbekov, M. B. Ismailov, T. A. Manko, and K. V. Kozis, "Study of the influence of rubber on stremgth properties of carbon plastic," *Space: Science & Technology,* vol. 28, no. 5, pp. 67-74, 2022.

[6] R. Novelline, *Squire’s Fundamentals of Radiology. Harvard University Press. 5th edition.* Cambridge: Harvard University Press Hardcover, 1997.

[7] A. M. Yermakhanova, A. K. Kenzhegulov, M. N. Meiirbekov, A. I. Samsonenko, and B. M. Baiserikov, "Study of radio transparency and dielectric permittivity of glass-aramid epoxy composites," *Eurasian Physical Technical Journal*, vol. 20, pp. 70-78, 2023.

[8] A. M. Yermakhanova, A. F. Sanin, M. N. Meiirbekov, and B. M. Baiserikov, "Investigation of dielectric and strength properties of composite materials. Review," *Complex Use of Mineral Resources,* vol. 322, no. 3, pp. 89-102, 2022.

[9] W. Li, W. Huang, Y. Kang, Y. Gong, Y. Ying, J. Yu, J. Zheng, L. Qiao, and S. Che, "Fabrication and investigations of G-POSS/ cyanate ester resin composites reinforced by silane-treated silica fibers," *Composites Science and Technology*, vol. 173, pp. 7-14, 2019.

[10] Z. Zhao, G. Zhou, Z. Yang, X. Cao, D. Jia, and Y. Zhou, "Direct ink writing of continuous SiO_2 fibre reinforced wave-transparent ceramics," *Journal of Advanced Ceramics*, vol. 9, pp. 403-412, 2020.

[11] A. T. Ospanali, A. K. Kenzhegulov, B. E. Zhumadilov, G. S. Suyundykova, B. S. Medyanova, G. Partizan, and B. A. Aliev, "Obtaining of carbon nanofibers based on polyacrylonitrile by the method of electrospinning," *Eurasian Physical Technical Journal,* vol. 33, no. 1(33), pp. 35-38, 2020.

[12] B. Baiserikov, A. Yermakhanova, M. Ismailov, A. Kenzhegulov, and B. Kenzhaliyev, "Study of prepregs lifetime based on epoxy resin with aromatic amine hardener," *Eurasian Physical Technical Journal*, vol. 20, no. 3(45), pp. 62-69, 2023.

[13] L. Tang, J. Zhang, Y. Tang, J. Kong, T. Liu, and J. Gu, "Polymer matrix wave-transparent composites: A review," *Journal of Materials Science & Technology*, vol. 75, pp. 225-251, 2021.

[14] Fiberglass and Its Properties, https://ktr.spb.ru/stati/stekloplastik-poliefirnaya-smola, accessed 29h May 2024.

[15] L. Yao, X. Wang, F. Liang, R. Wu, B. Hu, Y. Feng, and Y. Qiu, "Modeling and experimental verification of dielectric constants forthree-dimensional woven composites," *Composites Science and Technology,* vol. 68, pp. 1794-1799, 2008.

[16] High Energy Physics Group, https://hep.physics.illinois.edu/ home/serrede/P435/Lecture_Notes/Dielectric_Constants.pdf, 30th May 2024.

[17] U. Ponzi, M. Orefice, and P. Compagna, *Radio frequency (RF) transparent materials for feed towers: Guidelines.* Noordwijk: ERA requirements and standarts division, 1987.

[18] I. Choi, J. G. Kim, and I. S. Seo, "Aramid/epoxy composites sandwich structures for low-observable radomes," *Composites Science and Technology,* vol. 71, no. 14, pp. 1632-1638, 2011.

[19] I. Choi, D. Lee, and D. G. Lee, "Hybrid composite low-observable randome composed of Eglass/aramid/epoxy composite sandwich construction and frequency selective surface," *Composite Structures,* vol. 117, pp. 98-104, 2014.

[20] W. S. Chin, and D. G. Lee, "Binary mixture rule for predicting the dielectric properties of unidirectional E-glass/epoxy composite," *Composite Structures,* vol. 74, pp. 153-162, 2006.

[21] X. Xu, B. Zhang, K. Liu, L. Xing, D. Liu, and M. Bai, "Measurements and analysis of the dielectric properties of aramid/epoxy composites based on free space method under stress conditions," *Polymer Testing,* vol, 72, pp. 55-62, 2018.

[22] G. M. Tsangaris, and G. C. Psarras, "Permittivity and loss of composites of epoxy resin and kevlar fibres," *Advanced Composites Letters,* vol. 4, no. 4, pp. 125-128, 1995.

[23] X. Y. Xu, B. M. Zhang, K. Liu, M. Bai, and D. W. Liu, "Characterization of the dielectric properties of unidirectional aramid/epoxy composites at varying temperatures by rectangular waveguide method", *In 21st Intern. Conf. on Composite Materials*, 20 August 2017, pp. 1-6.

[24] A. M. Yermakhanova, B. M. Baiserikov, A. K. Kenzhegulov, M. N. Meiirbekov, and B. Y. Zhumadilov, "Study on methods to improve the mechanical properties of aramid/epoxy composites," *Journal of Elastomers & Plastics,* vol. 55, no. 2, pp. 331-346, 2023.

[25] Yu. V. Korickij and et al, *Electrical Materials Handbook,* Moscow: Energoatomizdat, 1974-1986.

[26] Yu. A. Gusev, *Fundamentals of dielectric spectroscopy,* Kazan: Kazan Federal University, 2008.

[27] Determination of the permittivity of a substance, http://bog5.in.ua/ lection/labrab/electrics/lr3_4.html, accessed 27th May 2023.

[28] G. Ginkin, *Handbook of Radio Engineering,* Moscow: State Energy Publishing House, 1948.

[29] X. Li, T. Liu, Y. Jiao, J. Dong, F. Gan, X. Zhao, and Q. Zhang, "Novel high-performance poly(benzoxazole-co-imide) resins with low dielectric constants and superior thermal stability derived from thermal rearrangement of ortho-hydroxy polyimide oligomers," *Chemical Engineering Journal,* vol. 359, pp. 641-651, 2019.

[30] L. Fumagalli, A. Esfandiar, R. Fabregas, S. Hu, P. Ares, A. Janardanan, Q. Yang, R. Boya, T. Taniguchi, K. Watanabe, G. Gomila, K. Novoselov, and A. Geim, "Anomalously low dielectric constant of confined water," *Science*, vol. 360, no. 6395, pp. 1339-1342, 2018.

[31] Y. Shen, Y. H. Lin, and C. W. Nan, "Interfacial effect on dielectric properties of polymer nanocomposites filled with core/shell-structured particles," *Advanced Functional Materials,* vol. 17, pp. 2405-2410, 2007.

[32] W. Du, Y. Zhou, Z. Yao, Y. Huang, C. He, L. Zhang, Y. H. He, L. Zhu, and X. Xu, "Active broadband terahertz wave impedance matching based on optically doped graphene-silicon hetero-junction," *Nanotechnology,* vol. 30, no. 19, p. 195705, 2019.

[33] Z. Man, P. Li, D. Zhou, Y. Wang, X. Liang, R. Zang, P. Li, Y. Zuo, Y. M. Lam, and G. Wang, "Two birds with one stone: FeS_2@C yolk–shell composite for high-performance sodium-ion energy storage and electromagnetic wave absorption," *Nano Letters,* vol. 20, pp. 3769-3777, 2020.

[34] A. Tang, F. Shen, B. Lan, Y. Ge, J. Li, and Y. Duan, In *Proceed. to the Sixth Symp. on Novel Photoelectronic Detection Technology and Application*, 3 December, 2020, p. 1145568.